INSTITUTE OF PHYSICS PUBLISHING SMART MATERIALS AND STRUCTURES
Smart Mater. Struct. **11** (2002) 947–955 PII: S0964-1726(02)53503-5

Effect of transformation volume contraction on the toughness of superelastic shape memory alloys

Wenyi Yan[1], **Chun Hui Wang**[2], **Xin Ping Zhang**[1] and **Yiu-Wing Mai**[1]

[1] Centre for Advanced Materials Technology, School of Aerospace, Mechanical and Mechatronic Engineering, The University of Sydney, NSW 2006, Australia
[2] Aeronautical and Maritime Research Laboratory, Defence Science and Technology Organisation, 506 Lorimer Street, Fishermans Bend, VIC 3207, Australia

Received 25 March 2002, in final form 29 July 2002
Published 7 October 2002
Online at stacks.iop.org/SMS/11/947

Abstract
Shape memory alloys (SMAs) exhibit two very important properties: shape memory phenomenon and superelastic deformation due to intrinsic thermoelastic martensitic transformation. To fully exploit the potential of SMAs in developing functional structures or smart structures in mechanical and biomechanical engineering, it is important to understand and quantify the failure mechanisms of SMAs. This paper presents a theoretical study of the effect of phase-transformation-induced volume contraction on the fracture properties of superelastic SMAs. A simple model is employed to account for the forward and reverse phase transformation with pure volume change, which is then applied to numerically study the transformation field near the tip of a tensile crack. The results reveal that during steady-state crack propagation, the transformation zone extends ahead of the crack tip due to forward transformation while partial reverse transformation occurs in the wake. Furthermore, as a result of the volume contraction associated with the austenite-to-martensite transformation, the induced stress-intensity factor is positive. This is in stark contrast with the negative stress-intensity factor achieved in zirconia ceramics, which undergoes volume expansion during phase transformation. The reverse transformation has been found to have a negligible effect on the induced stress-intensity factor. An important implication of the present results is that the phase transformation with volume contraction in SMAs tends to reduce their fracture resistance and increase the brittleness.

1. Introduction

Shape memory alloys (SMAs) are well known materials for their extraordinary behaviors: the shape memory effect and superelastic deformation. These behaviors are due to the intrinsic thermoelastic martensitic transformation at different temperatures. At some relatively low temperature and by subjection to an external force, the initial parent phase (austenite) can transform into a martensitic phase accompanying macroscopic deformation. Upon unloading, the material remains in a martensite state with residual strain. Then, when the material is heated to a certain temperature, the martensite can transform back to the initial austenite phase with the material returning to its initial shape. This is the shape memory effect, which is schematically shown in figure 1(a). For the same material, at some higher temperature, the transformed martensite due to loading can transform in reverse back to austenite during unloading while recovering a large amount of the prior deformation. This extraordinary recoverable deformation behavior is called superelasticity or pseudoelasticity, and is illustrated in figure 1(b) (Delaey *et al* 1974, Christian 1982).

Both the shape memory effect and the superelastic deformation have been exploited to design SMA-based

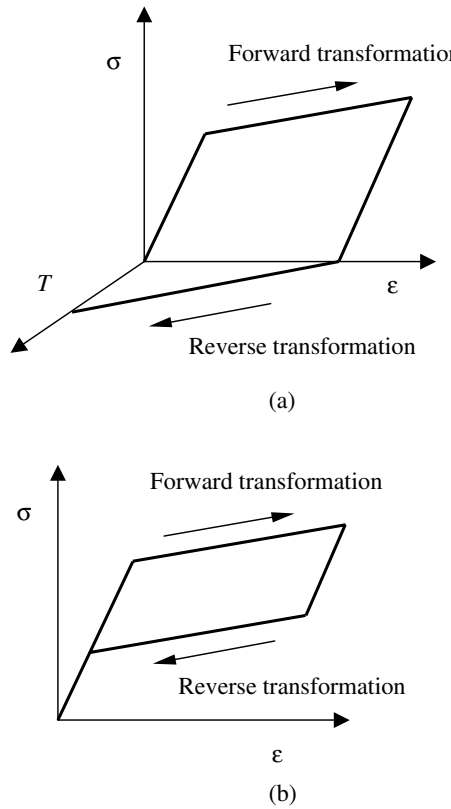

Figure 1. Illustration of the mechanisms of shape memory effect (a) and superelastic deformation (b).

functional structures and smart structures in mechanical and biomedical engineering, e.g. see Funakubo (1987), Birman (1997) and Van Humbeeck (1999), culminating in a number of commercial products. Examples include couplings and fasteners based on the shape memory effect and SMA vascular stents developed to reinforce blood vessels by applying either shape memory behavior or superelastic mechanisms. More recently SMA NiTi has been reported to exhibit super wear resistance due to its superelastic deformation and could be applied in tribological engineering (Li 2000). SMA-based composites (Porter *et al* 2000, Sittner and Stalmans 2000) are another important application.

Historically, research on SMAs has been developing in three stages. Early studies focused on the crystallography and thermodynamics of martensitic transformation, which were mainly carried out by material scientists and physicists. For example, Wechsler *et al* (1953) proposed a crystallographic habit plane theory on the formation of martensite, and Olson and Cohen (1982) studied the martensitic nucleation process. Due to the extraordinary mechanical behaviors of SMAs, mathematicians and mechanics scientists developed various constitutive laws to describe the stress–strain–temperature relations during forward and reverse transformation processes, which dominated the second stage research on SMAs in the past decade. For instances, Liang and Rogers (1990) developed a model based on the thermomechanical theory. Sun and Hwang (1993) established a micromechanics constitutive model based on an internal variable theory. Crystallographic theory of martensitic transformation was considered in the models of Patoor *et al* (1988) and Yan *et al* (1998). Detailed reviews on different constitutive transformation models can be found in Fischer *et al* (1996) and Birman (1997). The third stage or the current trend is to study the failure mechanisms of SMAs. With the significant increase in applications of SMAs as functional and smart structure materials, characterization of their failure mechanisms is rapidly gaining momentum. Some experimental works on the fatigue of SMAs have been reported, referring to the recent overview paper by Wilkes and Liaw (2000). However, quantitative and systematical studies on the failure mechanisms of SMAs are still lacking (McKelvey and Ritchie 1999, 2001).

With regard to the theoretical research on the failure of SMAs, Yi and Gao (2000) and Yi *et al* (2001) investigated the fracture toughness of SMAs under different far field loading conditions by applying Sun and Hwang's constitutive model (1993) in the regime of shape memory. No reverse transformation process was considered. Sun and Hwang's model was also applied by Stam and Van der Giessen (1995) to numerically study the effect of reversible transformation on crack growth in the regime of superelasticity. In Sun and Hwang's transformation model, the transformation volume strain was assumed to be much smaller than the transformation shear strain, and was thus ignored. However, recent experimental research by McKelvey and Ritchie (2001) indicated that the transformation volume strain in SMA NiTi might have great influence to hinder the transformation process near a fatigue crack tip with high triaxial stress.

Here it is important to note the similarities and differences between the phase transformation of SMAs and that of the zirconia ceramics. It is now well recognized that the stress-induced martensite transformation in zirconia ceramics involves predominately positive volumetric change, resulting in a reduction in the crack-tip stress-intensity factor (Hannink *et al* 2000, Kelly and Rose 2002), which in turn leads to an increase in the material fracture toughness. By contrast, the phase transformation in SMAs involves negative volumetric change. In the absence of any rigorous analysis, it may be expected that the phase transformation in SMAs would result in a completely opposite phenomenon: an increase in the crack-tip stress-intensity factor and thus a decrease in fracture toughness. It is the purpose of this paper to quantify the effect of volume contraction induced by austenite-to-martensite phase transformation on the fracture properties of SMAs. Both of the forward and reverse transformations, involving pure volume change, are considered in analyzing the crack growth driving force of a tensile crack in the superelastic regime. The variation of the stress-intensity factor during steady-state crack growth is investigated by determining the change of the stress-intensity factor due to forward and reverse transformation near a plane-strain crack tip. The evolution of the transformation zone during crack growth has been quantified using the finite element method.

2. Constitutive model

Phase transformation from austenite to martensite results in macroscopic deformation. This deformation can be separated into shear strain and volume strain. In the case of pure thermo-induced transformation (transformation is solely due to the change of temperature), martensitic twin structures

form to compensate the microscopic shear strains induced by different martensitic variants. On the macroscopic scale, the net shear strain is zero. By contrast, stress-induced martensitic transformation will result in a stress-biased macroscopic shear strain as well as a volume strain. As a first step towards studying the failure behavior of SMAs, only the transformation volume strain is considered in the present work; the effect of shear strain will be investigated separately. In this case, a simple constitutive law is proposed to describe the macroscopic stress–strain relation during the forward and reverse transformation process, which is described below.

Since only volume strain induced by phase transformation is considered, the transformation conditions are controlled by the mean stress, σ_m. The forward transformation occurs when the mean stress reaches a critical value, i.e.,

$$\sigma_m \equiv \tfrac{1}{3}\,\mathrm{tr}(\boldsymbol{\sigma}) = \sigma^c_{for}, \tag{1}$$

where $\boldsymbol{\sigma}$ denotes the stress tensor, and σ^c_{for} the critical forward transformation stress, which may be considered a material constant. In general, σ^c_{for} increases with temperature. The corresponding reverse transformation condition is

$$\sigma_m = \sigma^c_{rev}, \tag{2}$$

where σ^c_{rev} is another material constant, representing the critical reverse transformation stress, which also changes with temperature. To further simplify the following analysis, it is assumed that either forward or reverse transformation is fully complete once the corresponding critical mean stress is reached, i.e., the transformation strain will be added or removed instantly to the material point at critical transformation stresses. This transformation was termed supercritical transformation by Budiansky *et al* (1983). Supercritical transformation manifests instabilities and autocatalytic phenomena, which can be observed sometimes in SMAs, for example, see Miyazaki *et al* (1981). Based on this assumption, the progressive evolution of the transformation volume fraction is not considered. Therefore, it is possible to add or remove the stress-free transformation strain in numerical calculations by adopting the thermal strain concept, which is discussed in detail in the next section. The transformation strain tensor with pure volume strain can be represented by

$$\varepsilon^{tr} = \tfrac{1}{3}\boldsymbol{I}\varepsilon^{tr}_v, \tag{3}$$

where ε^{tr}_v is the transformation volume strain, and $\boldsymbol{I}$ denotes a unit tensor. The total strain ε consists of the elastic strain ε^{el} and the transformation strain ε^{tr}:

$$\varepsilon = \varepsilon^{tr} + \varepsilon^{el}. \tag{4}$$

The elastic strain is given by the isotropic Hooke's law:

$$\boldsymbol{\sigma} = \boldsymbol{M} : \varepsilon^{el}, \tag{5}$$

where $\boldsymbol{M}$ is the elastic stiffness tensor. It is assumed that the austenite and the martensite have the same elastic constants; the effect of elastic mismatch will be considered in the future. Physically, in the case of copper-based SMAs, the difference of the Young's modulus between the martensite and the austenite is negligibly small. By contrast, for binary NiTi SMAs the

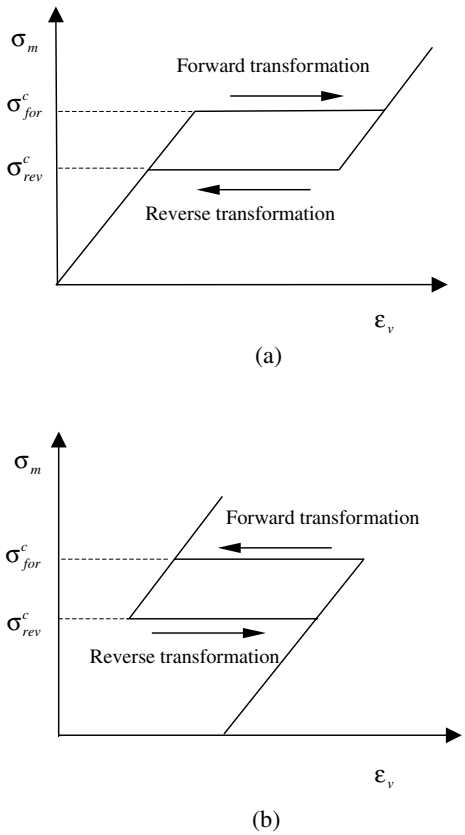

Figure 2. A schematic illustration of the relation between the mean stress and the total volume strain for the transformation model with pure volume change: (a) transformation volume expansion ($\varepsilon^{tr}_v > 0$); (b) transformation volume contraction ($\varepsilon^{tr}_v < 0$).

Young's modulus of the martensite is about one-third to one-half of the Young's modulus of the austenite; see Hodgson *et al* (1991). Since the transformation strain rate is much greater than the elastic strain rate during a transformation process, for either forward transformation or reverse transformation, the elastic mismatch between austenite and martensite can only have a very limited effect on the macroscopic deformation of NiTi SMAs. On the other hand, while this difference can be readily incorporated in the theoretical model, more elaborate experiments would then be required to identify the necessary material constants; see the discussion in Yan *et al* (2002).

In the present simple model, the forward and reverse transformation processes are described by three material parameters only: σ^c_{for}, σ^c_{rev} and ε^{tr}_v. The relation of the mean stress and the total volume strain $\varepsilon_v\,(=\ \varepsilon^e_v + \varepsilon^{tr}_v)$ is schematically illustrated in figure 2, indicating in figure 2(a) a volume expansion during the austenite-to-martensite transformation and in figure 2(b) volume contraction during austenite-to-martensite transformation. Many SMAs contract slightly during the forward austenite-to-martensite transformation process. For example, the transformation volume strain, ε^{tr}_v, for CuAlNi SMA equals -0.37% according to the calculation of Fang *et al* (1999). For typical SMA NiTi the volume strain is about -0.39% according to the measurement by Holtz *et al* (1999). By contrast, the tetragonal-to-monoclinic martensitic transformation in zirconia ceramics results in a volume expansion of 4%.

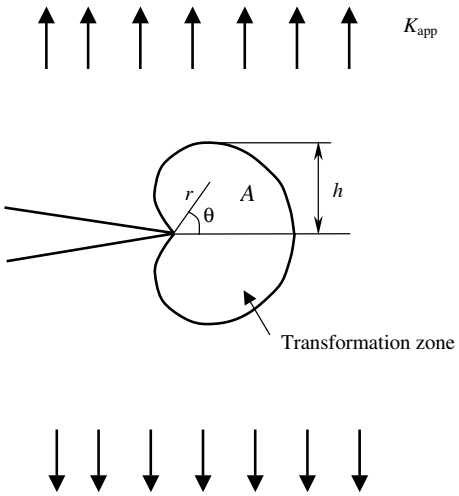

Figure 3. Schematic illustration of transformation zone near a stationary crack tip.

3. Toughness analysis

3.1. Analysis of crack-tip stress-intensity factor

Figure 3 illustrates a stationary semi-infinite plane-strain crack in a superelastic SMA, which is initially in the austenite state. Under mode I loading condition, martensitic transformation occurs around the crack tip. The transformation zone occupied by the transformed martensite is denoted by A. In the present study, the half-height of the transformation zone, h, near a stationary crack tip, is chosen as a reference length scale, similar to the approach employed in analyzing transformation toughening of zirconia-contained ceramics.

The value of the transformed zone size h is assumed to be much smaller than the crack length. In other words, this is a small-scale transformation problem. As the plastic yield strength is normally greater than the critical transformation stress, it is expected that plastic deformation zone is much smaller than the transformation zone, referring to recent numerical study by Yan *et al* (2002). Thus, linear elastic fracture mechanic theory is adequate for this problem. The stress field remote from the transformation zone, which controls the transformation process, is given by

$$\sigma_{ij} = \frac{K_{app}}{\sqrt{2\pi r}} f_{ij}(\theta) \qquad (r \to \infty) \tag{6}$$

where K_{app} is the applied remote stress-intensity factor. The functions $f_{ij}(\theta)$ are given in many reference books, such as Anderson (1995). Consequently the problem can be analyzed by a boundary layer approach in which the stress state given by equation (6) is imposed as the far field for a semi-infinite crack.

Due to phase transformation, the stress field very close to the crack tip is disturbed, resulting in a different magnitude of the crack-tip stress-intensity factor, K_{tip}, while the stress field at the crack tip is still given a similar form as equation (6), i.e.,

$$\sigma_{ij} = \frac{K_{tip}}{\sqrt{2\pi r}} f_{ij}(\theta) \qquad (r \to 0). \tag{7}$$

It is K_{tip} that controls the fracture process, which is generally different from the applied stress-intensity factor, K_{app}. The difference is the stress-intensity factor induced by the transformation, K_{tran}. Hence, we have

$$K_{tip} = K_{app} + K_{tran}. \tag{8a}$$

The parameter K_{tran} represents the change in crack growth driving force in the presence of phase transformation. At the onset of crack growth, K_{tip} is equal to the material intrinsic toughness, K_{IC} and the value of K_{app} is normally taken to be the measured (or apparent) toughness or the crack resistance, see Foote *et al* (1986). Thus,

$$K_{app} = K_{IC} - K_{tran}. \tag{8b}$$

If $K_{tran} < 0$, as in the case of stress-induced martensitic transformation in zirconia ceramics, phase transformation results in an increase in the apparent toughness of the materials. On the other hand, the apparent toughness of the material would decrease if $K_{tran} > 0$, which is the case in the present context, as detailed below.

Once the transformation zone is determined, K_{tran} can be evaluated by (Hutchinson 1974, McMeeking and Evans 1982)

$$K_{tran} = \frac{E\varepsilon_v^{tr}}{6\sqrt{2\pi}(1-\nu)} \int\int_A r^{-3/2} \cos\left(\frac{3}{2}\theta\right) \mathrm{d}A \tag{9}$$

where E and ν are the material's Young modulus and Poisson ratio, respectively. For a stationary crack subjected to monotonically increasing K_{app}, only forward transformation occurs. In this case, McMeeking and Evans (1982) and Budiansky *et al* (1983) proved $K_{tran} = 0$, i.e., $K_{tip} = K_{app}$. As soon as crack growth occurs, K_{tran} is no longer zero.

An asymptotic solution for the half-height h of the transformation zone, defined in figure 3, can be obtained based on the far-field stress field equation (6) (see Budiansky *et al* 1983),

$$h = \frac{\sqrt{3}(1+\nu)^2}{12\pi} \left(\frac{K_{app}}{\sigma_{for}^c}\right)^2. \tag{10}$$

In the present study, the finite element approach will be applied to determine the transformation zone and transformation-induced stress-intensity factor K_{tran}. The asymptotic solution of the transformation zone size h from equation (10), which is determined by K_{app} and σ_{for}^c, is used as a reference length scale in our parametric study.

3.2. Dimensional analysis

According to the above analysis, the change of the apparent toughness of the materials due to transformation can be quantified by calculating K_{tran} from equation (9). Given the material's elastic property, the functional dependence of K_{tran} on the independent parameters is

$$K_{tran} = f(\Delta a, K_{app}, \varepsilon_v^{tr}, \sigma_{for}^c, \sigma_{rev}^c) \tag{11}$$

where Δa is the crack advance. There are two fundamental dimensional units in the present problem, i.e., force and length. According to dimensional analysis theory, see Anderson (1995), the following dimensionless function is available:

$$\frac{K_{tran}}{K_{app}} = f\left(\frac{\Delta a}{h}, \varepsilon_v^{tr}, \frac{\sigma_{rev}^c}{\sigma_{for}^c}\right). \tag{12}$$

Therefore, the normalized transformation-induced stress intensity factor, K_{tran}/K_{app}, is completely determined by the relative crack advance, $\Delta a/h$, the transformation volume strain, ε_v^{tr}, and the transformation stress ratio, $\sigma_{rev}^c/\sigma_{for}^c$. Based on this equation, the influence of transformation parameters on material toughness will be investigated in the next section.

3.3. Finite element analysis

As reverse transformation will occur in the wake of an advancing crack, no closed-form analytical solution can be obtained for the transformation zone size. Instead, the finite element method is employed in the present investigation, using the software package ABAQUS (1998).

The forward and reverse transformation model described in section 2 is implemented through user subroutines USDFLD and UEXPAN in ABAQUS without using the user-defined material subroutine UMAT. The transformation statement of a material point is determined by a state variable defined in subroutine USDFLD. The stress-free transformation strain is added or removed at the material point as a thermal strain in subroutine UEXPAN. Such an approach was successfully applied to numerically simulate transformation problems of ceramics, see Yan *et al* (1997).

The finite element model for a semi-infinite crack is shown in figure 4. Here a plane-strain problem is considered, which is an appropriate approximation for most real cracks. A remote model-I field, K_{app}, is applied on the boundary far away from the crack tip. Due to symmetry, only a half geometrical model is simulated. A total of 2941 eight-node quadrilateral elements are employed in the finite element model. Fine meshes are built near the crack tip. For the purpose of our present study, it is not necessary to use special elements to simulate the stress singularity at the crack tip. The node release technique is applied to simulate crack growth. In each step, two nodes are released to represent crack advance of the length of one element side. In order to accurately simulate the supercritical transformation process, special effort is made to control the increment time. Generally, one-step calculation involves about 250 increments. Therefore, significant computing time is required to simulate crack growth. For example, it takes about 40 CPU hours to run 100 steps in a Compaq ES45 supercomputer.

Referring to equation (8*b*), due to the change of K_{tran} during crack growth, physically, K_{app} should be adjusted correspondingly in order to keep the crack growing quasi-statically. For example, in the case of $K_{tran} < 0$ in zirconia ceramics, K_{app} should increase with crack growth while K_{app} should decrease if $K_{tran} > 0$. However, considering that K_{tran} might reach a constant steady-state value after a relatively short crack growth (see the results in the next section) and that the constant steady-state value is more significant in the present crack growth simulation, no special crack growth criterion is introduced. Instead, the crack growth is assumed to occur under constant remote K_{app}. Therefore, the effect of transformation on the apparent toughness can still be theoretically investigated without knowing the intrinsic toughness of the material, K_{IC}. Such a technique has also been applied in the toughness study of zirconia ceramics, for example see Budiansky *et al* (1983).

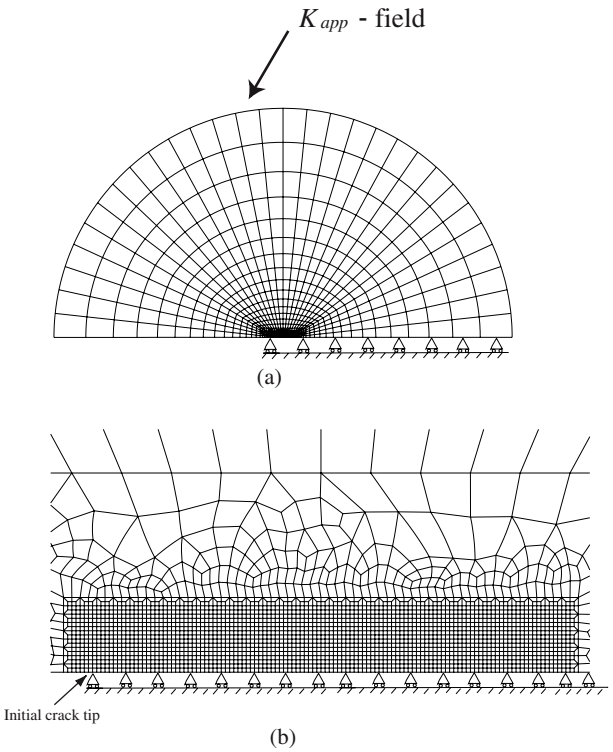

Figure 4. Finite element model for the growth of a semi-infinite plane-strain crack in a superelastic SMA subjected to remote K_I field force: (a) entire finite element mesh and boundary conditions; (b) fine mesh near the crack tip.

Based on the theory of fracture mechanics, the remote mode I stress intensity, K_{app}, is applied by imposing a displacement field along the boundary of the finite element model:

$$u_x = \frac{K_{app}}{2\mu}\sqrt{\frac{r}{2\pi}}(3-4\nu-\cos\theta)\cos\frac{\theta}{2}$$
$$u_y = \frac{K_{app}}{2\mu}\sqrt{\frac{r}{2\pi}}(3-4\nu-\cos\theta)\sin\frac{\theta}{2} \tag{13}$$

where $\mu = \frac{E}{2(1+\nu)}$ is material's elastic shear modulus. For NiTi SMA, the elastic Young modulus, E, and Poisson ratio, ν, are respectively chosen as 62 GPa and 0.3 in the present investigation.

4. Results and discussion

The transformation field near the crack tip is firstly studied. In this case, the remote applied model-I stress intensity factor, K_{app}, is chosen to be 20 MPa m$^{1/2}$. The transformation volume strain, ε_v^{tr}, is -0.39%, which corresponds to NiTi SMAs. Assuming that the austenite phase is in the stress-free state, stress-induced transformation occurs around the stationary crack tip, as shown in figure 5(a). The parameter FV2 in our numerical study represents the average volume fraction of the transformed martensite in an element. FV2 = 1.0 means that all the material within the element has been transformed into martensite, and FV2 = 0.0 means that the material in this element is in austenite. Therefore, the distribution of the parameter FV2 represents the distribution of the martensite

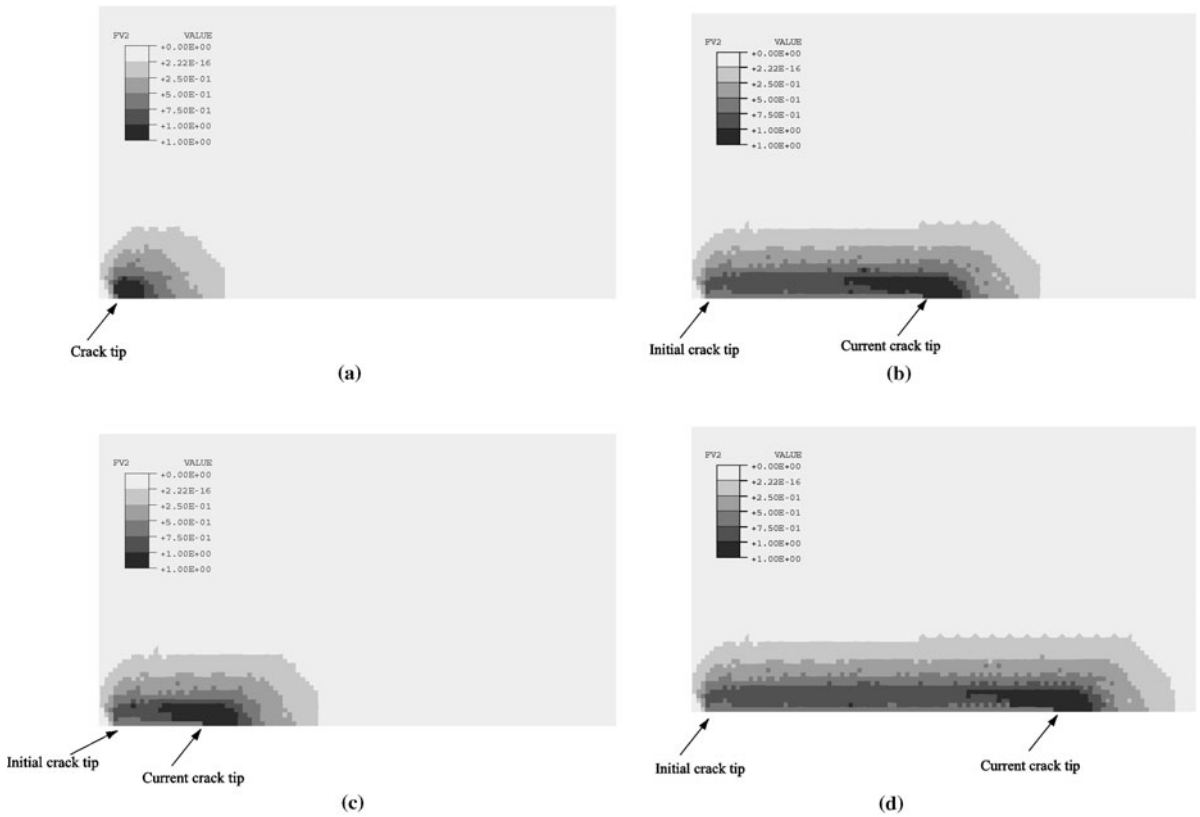

Figure 5. Tranformation field near the crack tip at different stages of crack growth: (a) $\Delta a/h = 0.0$; (b) $\Delta a/h = 1.48$; (c) $\Delta a/h = 3.70$; (d) $\Delta a/h = 5.93$.

phase, i.e., it indicates the transformation field. Figure 5(a) shows that there exists a small fully transformed zone with FV2 = 1.0 just in front of the stationary crack tip with partly transformed zone enclosing it. The width of the fully transformed zone is about one-third of the half-height of the whole transformation zone, h. Figures 5(b)–(d) shows the variation of the transformation field near the growing crack tip at different stages from $\Delta a/h = 1.48$ to 5.93. With crack growth, these pictures show that the transformation zone extends along the crack plane. The height of the transformation zone remains the same. Due to the unloading in the wake of the crack tip, reverse transformation occurs in this region. However, because of the residual tensile stress field resulting from volume contraction during forward transformation, reverse transformation cannot occur completely in the wake, leaving a layer of partial martensite and partial austenite.

After obtaining the transformation field, the stress intensity factor, K_{tran}, is then calculated according to equation (9). The influence of the transformation strain, ε_v^{tr}, and the transformation stress ratio, $\sigma_{rev}^c/\sigma_{for}^c$, on the normalized transformation-induced stress-intensity factor, K_{tran}/K_{app}, during crack growth have been investigated (see equation (11)). Figure 6 shows the results of the normalized transformation-induced stress intensity with crack growth for different transformation volume strains under the same transformation stress ratio. It is clear that the numerical result is close to zero before crack advance for all the three cases with different values of transformation volume strain, ε_v^{tr}, which is consistent with theoretical analysis; see McMeeking and Evans (1982) and Budiansky *et al* (1983). More importantly, figure 6 shows that the transformation-induced stress intensity is positive once the crack advances. Referring to equation (8*a*), thus, the effective stress intensity factor near the crack tip, K_{tip}, increases. This implies that crack growth would occur at higher driving force. In other words, the apparent toughness of the material would decrease, referring to equation (8*b*). It is also clear K_{tran}/K_{app} approaches asymptotically to a constant value after the crack extension exceeds about five times the half-height of the transformation zone. Figure 6 also indicates that the steady value of the transformation-induced stress intensity increases with the amplitude of the transformation volume strain. The maximum value of K_{tran}/K_{app} is about 17% for $\varepsilon_v^{tr} = -0.60\%$; it is about 12% for $\varepsilon_v^{tr} = -0.39\%$. The increase of the crack-tip effective stress intensity is due to the transformation volume contraction, which results in a tensile stress field around the crack tip, and as a result, K_{tip} increases.

The influence of the transformation stress ratio, $\sigma_{rev}^c/\sigma_{for}^c$, on the normalized transformation-induced stress-intensity factor is shown in figure 7. The transformation volume strain, ε_v^{tr}, is chosen to be the same, -0.39%, in all three cases with different values of $\sigma_{rev}^c/\sigma_{for}^c$. It can be seen that the transformation-induced stress-intensity factor increases with decreasing $\sigma_{rev}^c/\sigma_{for}^c$ during crack growth although the dependence is not significant. Referring to figure 2(b), a smaller value of $\sigma_{rev}^c/\sigma_{for}^c$ led to a larger area of hysteresis loop. Figure 7 further indicates that the dependence of the transformation stress ratio on the transformation-induced stress-intensity factor is not significant. This can be explained by the fact that reverse transformation can only partly occur

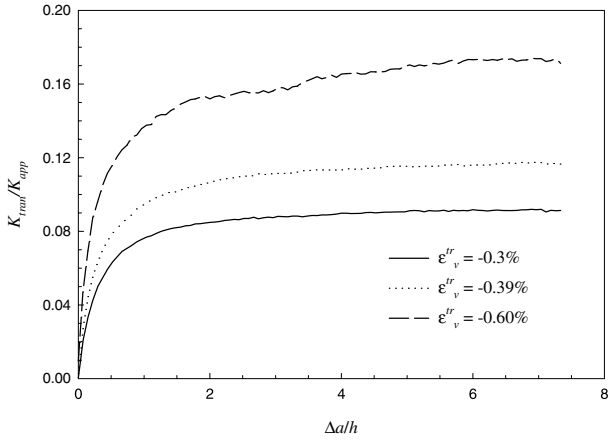

Figure 6. Variation of the normalized transformation-induced stress-intensity factor with normalized crack growth for different transformation volume strains; in all cases, $\sigma^c_{rev}/\sigma^c_{for} = 0.49$.

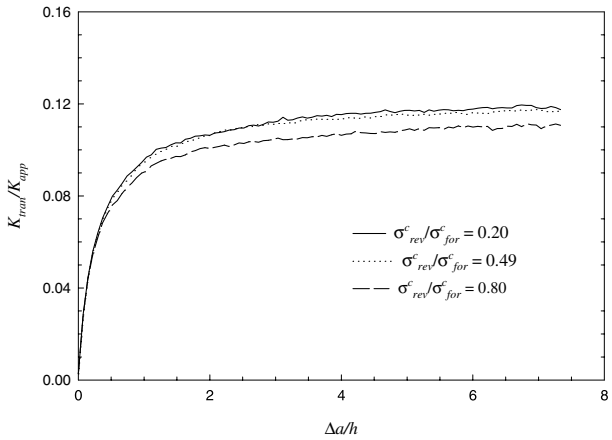

Figure 7. Influence of transformation stress ratio on the normalized transformation-induced stress intensity during crack growth; in all cases, $\varepsilon^{tr}_v = -0.39\%$.

in the wake of the crack tip; see figure 5, which results as a minor effect of reverse transformation on the change of the stress-intensity factor as shown below.

In order to investigate the influence of reverse transformation on the toughness in SMAs, a case with irreversible transformation, i.e., no reverse transformation is allowed, is studied. Physically, irreversible austenite-to-martensite transformation occurs in SMAs at lower temperature, at which martensite phase can be stable after removing external force. The calculated transformation-induced stress-intensity factors are shown in figure 8 together with that corresponding to reversible transformation. The results clearly indicate that there is little difference between the results for reversible transformation and irreversible transformation. Hence, the influence of reverse (volume) transformation on the crack toughness is negligible. Referring to figure 3, a possible reason might be that the reverse transformation can only occur partly in the wake of the advancing crack tip.

Considerable analytical studies have been carried out on the toughness induced by irreversible transformation volume expansion in zirconia-containing ceramics. For example, Becher and Rose (1992) predicted

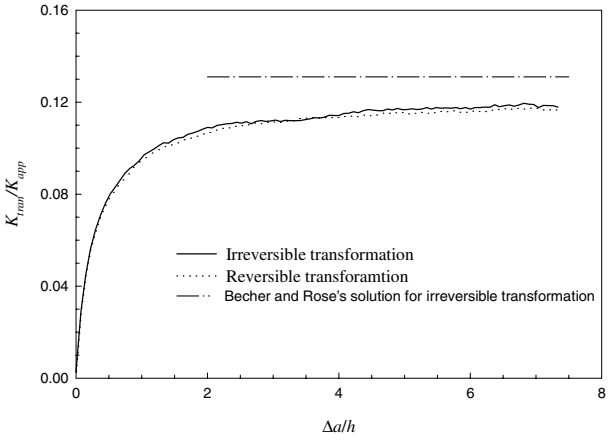

Figure 8. Influence of reverse transformation on the normalized transformation-induced stress-intensity factor with $\sigma^c_{rev}/\sigma^c_{for} = 0.49$ and $\varepsilon^{tr}_v = -0.39\%$.

$$\frac{K_{tran}}{K_{app}} = 0.044\frac{(1+v)E\varepsilon^{tr}_v}{(1-v)(\sigma^c_{for} - \sigma^*)}, \tag{14}$$

where $\sigma^* = \frac{(1+v)Ef\varepsilon^{tr}_v}{30(1-v)}$. Although this result was derived for irreversible volume expansion transformation, it can be adapted to deal with irreversible volume contraction transformation in SMAs, provided that ε^{tr}_v is taken to be negative. For the case when $\varepsilon^{tr}_v = -0.39\%$, σ^* is calculated to be -14.97 MPa. Consequently, equation (14) yields a ratio of 13.1%, which is depicted by the dashed–dotted curve in figure 8. This analytical solution is close to the present numerical result of 12%.

As mentioned in section 1, extensive effort has been directed towards the research of the transformation-induced toughness in zirconia-containing ceramics. Comparing to the martensitic transformation in SMAs, one of the major differences is that the transformation from austenite to martensite results in volume expansion in zirconia, i.e., the transformation volume strain, ε^{tr}_v, is positive in zirconia. For the sake of a comparative study, the effect of transformation volume expansion with reversible transformation on material toughness has also been investigated. For this purpose, only the sign of the value of ε^{tr}_v needs to be changed in the numerical calculations. Some of the results with different amplitude of the transformation volume strain are shown in figure 9, which indicates that the normalized transformation-induced stress intensity is negative in all the cases. Referring to equation (8*a*), the resulting effective stress-intensity factor near the crack tip, K_{tip}, would decrease, which is consistent with earlier research on zirconia. The level of the toughness increment increases with the amplitude of the transformation volume strain.

Referring to figure 6, the amplitude of the normalized transformation-induced stress-intensity factor, K_{tran}/K_{app}, for volume-contracting transformation is much greater than that corresponding to volume-expanding transformation. For example, the value of K_{tran}/K_{app} is about 12% with $\varepsilon^{tr}_v = -0.39\%$, while it is only -2.7% with $\varepsilon^{tr}_v = 0.39\%$. According to the formula of equation (9), the sign of ε^{tr}_v does not change the amplitude of the integrand to evaluate K_{tran}. The integral area, i.e. the transformation zone, must be greatly different in these two cases. Figure 10 demonstrates the transformation

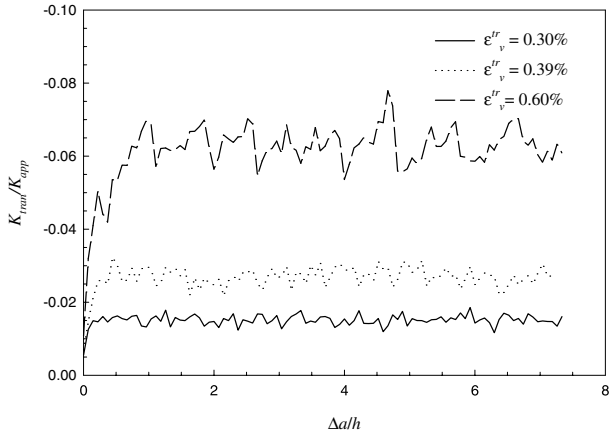

Figure 9. Effect of transformation volume expansion on the normalized transformation-induced stress intensity factor with different amplitude; in all the cases, $\sigma^c_{rev}/\sigma^c_{for} = 0.49$.

fields for transformation volume expansion near the crack tip for a stationary crack and the crack with normalized crack growth $\Delta a/h = 3.70$. In this case, the transformation volume strain, ε^{tr}_v, is taken as 0.39% and the applied far-field stress-intensity factor, K_{app}, is 20 MPa m$^{1/2}$. Figure 10(b) indicates clearly that the reverse transformation is carried out very well in the wake of the advancing crack tip, in contrast to figure 5(c) for the case of volume-contracting transformation. As stated by Evans and Cannon (1986), transformation volume expansion in zirconia creates a residual compressive field. The transformation zone would easily reverse when the applied loads are removed. By contrast, transformation volume contraction in SMAs creates a residual tensile field, which limits the reverse transformation. As a consequence, reverse transformation can only slightly occur in the wake of the advancing crack in SMAs.

The influence of reverse transformation in the case of volume-expanding transformation is further demonstrated in figure 11. The normalized transformation-induced stress-intensity factors with normalized crack growth are depicted for both reversible transformation with $\sigma^c_{rev}/\sigma^c_{for} = 0.49$ and irreversible transformation with the same critical austenite-to-martensite transformation stress. The solid curve for reversible transformation is much lower than the dotted curve for irreversible transformation in the stable stage. The influence of reverse transformation can be quantified by the ratio of the transformation-induced stress-intensity factor due to reversible volume-expanding transformation to that due to irreversible transformation. In the present case, the ratio is about 0.16 according to figure 11. Evans and Cannon (1986) estimated a transformation zone near the advancing crack tip in reversible volume-expanding transformation material based on a linear elastic stress field. Their transformation zone in the wake is much larger than our numerical result. Their predicted ratio of the transformation-induced stress intensity factors is $(1 - \sigma^c_{rev}/\sigma^c_{for}) = 0.51$, which is much higher than 0.16. This difference could be due to simplification introduced by Evans and Cannon in deriving their analytical solution. Further studies are required to clarify this issue.

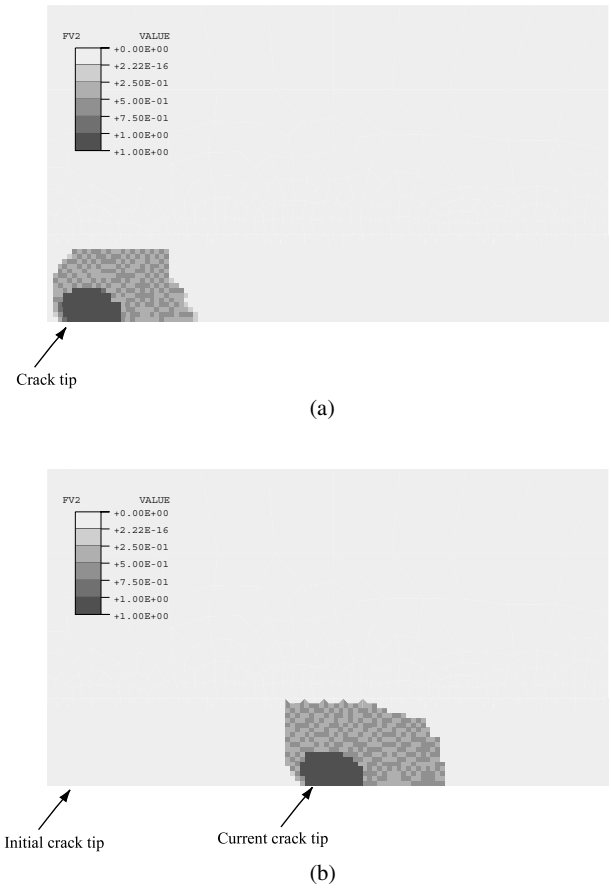

Figure 10. Tranformation field near the crack tip for $\varepsilon^{tr}_v = 0.39\%$ at different stages of crack growth: (a) $\Delta a/h = 0.0$; (b) $\Delta a/h = 3.70$.

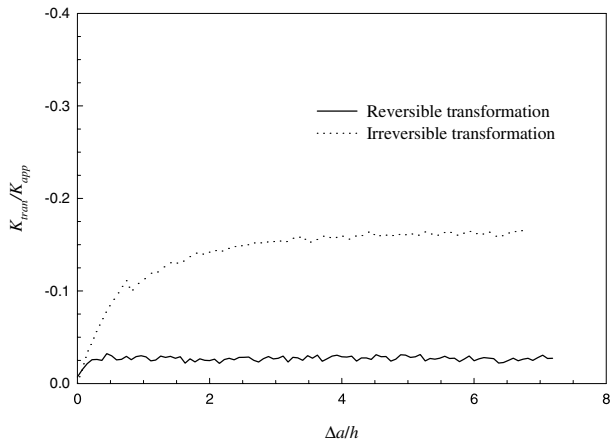

Figure 11. Influence of reversible tranformation on the normalized tranformation-induced stress intensity factor in the case of transformation volume expansion with $\varepsilon^{tr}_v = 0.39\%$.

5. Conclusions

The effect of volume-contracting transformation on the toughness of superelastic SMAs has been investigated by analyzing the transformation-induced stress-intensity factor for a quasi-static advancing crack. Based on the present results, the following conclusions can be drawn.

(1) Although the transformation volume contraction strain is less than a half percent in SMAs, it can increase the effective stress intensity near an advancing crack tip to over 10%. Therefore, transformation volume contraction reduces the toughness of SMAs.
(2) Reverse transformation has negligible effect on transformation-induced stress-intensity factor for SMAs due to the fact that reverse transformation can only partially occur in the wake of an advancing crack tip.
(3) For the materials with volume-expanding transformation, transformation can increase the toughness of the material. However, reverse transformation would greatly reduce the effect as in this case reverse transformation can be carried out very well in the wake.

Acknowledgments

This work was financially supported by the ARC Large Research Grant (A10009166). Most of the calculations were carried out at the National Facility of the Australian Partnership for Advanced Computing through an award under the Merit Allocation Scheme to WY. YWM wishes to thank the Australian Research Council for the award of a Federation Fellowship tenable at the University of Sydney.

References

ABAQUS 1998 *Version 5.8* (Providence, RI: HKS)
Anderson T L 1995 *Fracture Mechanics: Fundamentals and Applications* 2nd edn (Boca Raton, FL: Chemical Rubber Company)
Becher P F and Rose L R F 1992 Toughening mechanism in ceramic systems *Encyclopedia of Materials Science and Technologies* vol 11, ed R W Cahn, P Haasen and E J Kramer (Weinheim: VCH Publications) ch 8
Birman V 1997 Review of mechanics of shape memory alloy structures *Appl. Mech. Rev.* **50** 629–45
Budiansky B, Hutchinson J W and Lambropoulos J C 1983 Continuum theory of dilatant transformation toughening in ceramics *Int. J. Solids Struct.* **19** 337–55
Christian J M 1982 Deformation by moving interfaces *Metall. Trans.* A **13** 509–38
Delaey L, Krishnan R V, Tas H and Warlimot H 1974 Review thermoelasticity, pseudoelasticity and the memory effects associated with martensitic transformations *J. Mater. Sci.* **9** 1521–55
Evans A G and Cannon R M 1986 Toughening of brittle solids by martensitic transformations *Acta Metall.* **34** 761–800
Fang D-N, Lu W, Yan W, Inoue T and Hwang K-C 1999 Stress–strain relation of CuAlNi SMA single crystal under biaxial loading—constitutive model and experiments *Acta Mater.* **47** 269–80
Fischer F D, Sun Q-P and Tanaka K 1996 Transformation-induced plasticity (TRIP) *Appl. Mech. Rev.* **49** 317–64
Foote R M, Mai Y-W and Cotterell B 1986 Crack growth resistance curves in strain-softening materials *J. Mech. Phys. Solids* **34** 593–607
Funakubo H 1987 *Shape Memory Alloys* (New York: Gordon and Breach)
Hannink R H J, Kelly P M and Muddle B C 2000 Transformation toughening in zirconia-containing ceramics *J. Am. Ceram. Soc.* **83** 461–87
Hodgson D E, Wu M H and Biermann R J 1991 Shape memory alloys *Metals Handbook* vol 2, 10th edn (Cleveland, OH: American Society for Metals) pp 897–902
Holtz R L, Sadananda K and Imam M A 1999 Fatigue thresholds of Ni–Ti alloy near the shape memory transition temperature *Int. J. Fatigue* **21** s137–45
Hutchinson J W 1974 On steady quasi-static crack growth *Harvard University Report* Division of Applied Sciences, DEAP p S-8
Kelly P M and Rose L R F 2002 The martensitic transformation in ceramics—its role in transformation toughening *Mater. Sci.* **47** 463–557
Li D Y 2000 Exploration of TiNi shape memory alloy for potential application in a new area: tribological engineering *Smart Mater. Struct.* **9** 717–26
Liang C and Rogers C A 1990 One-dimensional thermomechanical constitutive relations for shape memory materials *J. Intell. Mater. Syst. Struct.* **1** 207–34
McKelvey A L and Ritchie R O 1999 Fatigue-crack propagation in Nitinol, a shape-memory and superelastic endovascular stent material *J. Biomed. Mater. Res.* **47** 301–8
McKelvey A L and Ritchie R O 2001 Fatigue-crack growth behavior in the superelastic and shape-memory alloy Nitinol *Metall. Mater. Trans.* A **32A** 731–43
McMeeking R M and Evans A G 1982 Mechanics of transformation-toughening in brittle materials *J. Am. Ceram. Soc.* **65** 242–46
Miyazaki S, Imai T, Otsuka K and Suzuki Y 1981 Lueders like deformation observed in the transformation pseudoelasticity of a Ti–Ni alloy *Scr. Metall.* **15** 853–6
Olson G B and Cohen M 1982 Theory of martensitic nucleation: a current assessment *Solid–Solid Transformations* ed H I Aaronson *et al* (Warrendale, PA: Metallurgical Society of AIME) pp 1145–64
Patoor E, Eberhardt A and Berveiller M 1988 Thermomechanical behavior of shape memory alloys *Arch. Mech.* **40** 775–94
Porter G A, Liaw P K, Tiegs T N and Wu K H 2000 Ni–Ti SMA-reinforced Al composites *JOM—J. Miner. Met. Mater. Soc.* **52** 52–6
Sittner P and Stalmans R 2000 Developing hybrid polymer composites with embedded shape-memory alloy wires *JOM—J. Miner. Met. Mater. Soc.* **52** 15–20
Stam G and Van der Giessen E 1995 Effect of reversible phase transformation on crack growth *Mech. Mater.* **21** 51–71
Sun Q-P and Hwang K-C 1993 Micromechanics modeling for the constitutive behavior of polycrystalline shape memory alloys *J. Mech. Phys. Solids* **41** 1–33
Van Humbeeck J 1999 Non-medical applications of shape memory alloys *Mater. Sci. Eng.* A **273–275** 134–48
Wechsler M S, Lieberman D S and Read T A 1953 On the theory of the formation of martensite *AIME Trans. J. Metals* **197** 1503–15
Wilkes K E and Liaw P K 2000 The fatigue behavior of shape-memory alloys *JOM—J. Miner. Met. Mater. Soc.* **52** 45–50
Yan W, Reisner G and Fischer F D 1997 Micromechanical study on the morphology of martensite in constrained zirconia *Acta Mater.* **45** 1969–76
Yan W, Sun Q-P and Hwang K-C 1998 A generalized micromechanics constitutive theory of single crystal with thermoelastic martensitic transformation *Sci. China* A **28** 275–82
Yan W, Wang C H, Zhang X P and Mai Y-W 2002 A combined constitutive model for transformation and plasticity in superelastic shape memory alloys, submitted
Yi S and Gao S 2000 Fracture toughening mechanism of shape memory alloys due to martensite transformation *Int. J. Solids Struct.* **37** 5315–27
Yi S, Gao S and Shen L 2001 Fracture toughening mechanism of shape memory alloys under mixed-mode loading due to martensite transformation *Int. J. Solids Struct.* **38** 4463–76